Journal of Solid State Chemistry 181 (2008) 2092–2098

Contents lists available at ScienceDirect

Journal of Solid State Chemistry

journal homepage: www.elsevier.com/locate/jssc

Synthesis and crystal structure of the high-pressure iron borate α-FeB_2O_4

Johanna S. Knyrim [a], Hubert Huppertz [b,*]

[a] Department Chemie und Biochemie, Ludwig-Maximilians-Universität München, Butenandtstrasse 5-13, D-81377 München, Germany
[b] Institut für Allgemeine, Anorganische und Theoretische Chemie, Leopold-Franzens-Universität Innsbruck, Innrain 52a, A-6020 Innsbruck, Austria

ARTICLE INFO

Article history:
Received 21 March 2008
Received in revised form
8 May 2008
Accepted 12 May 2008
Available online 18 May 2008

Keywords:
High-pressure
Multianvil
Crystal structure
Borate

ABSTRACT

The high-pressure iron borate α-FeB_2O_4 was synthesized under high-pressure and high-temperature conditions in a Walker-type multianvil apparatus at 7.5 GPa and 1100 °C. The monoclinic iron borate crystallizes with eight formula units in the space group $P2_1/c$ with the lattice parameters $a = 715.2(2)$, $b = 744.5(2)$, $c = 862.3(2)$ pm, and $\beta = 94.71(3)^\circ$. The compound is built up exclusively from corner-sharing BO_4-tetrahedra, isotypic to the monoclinic phases β-$SrGa_2O_4$, $CaAl_2O_4$-II, and $CaGa_2O_4$. Additionally, the structure is closely related to the orthorhombic compound $BaFe_2O_4$. The structure consists of layers of six-membered rings, which are interconnected to a three-dimensional network. The iron cations are coordinated by six and seven oxygen atoms. Next to synthesis and crystal structure of the new high-pressure borate, structural coherences to other structure types are discussed.

1. Introduction

Recent studies in high-pressure/high-temperature chemistry of borates revealed a large variety of new polymorphs like β-MB_4O_7 (M = Mn [1], Ni [1], Cu [1], Zn [2], Ca [3], Hg [4]), the rare-earth meta-oxoborates δ-$RE(BO_2)_3$ (RE = La, Ce) [5,6], as well as a new non-centrosymmetric modification δ-BiB_3O_6 of the well-characterized nonlinear optical material bismuth triborate [7]. Furthermore, a couple of new compositions could be realized in the compounds β-SnB_4O_7 [8], $Pr_4B_{10}O_{21}$ [9], and CdB_2O_4 [10]. The borates $RE_4B_6O_{15}$ (RE = Dy, Ho) [11–13], α-$RE_2B_4O_9$ (RE = Sm–Ho) [14–16], and the recently found HP-NiB_2O_4 [17] showed the interesting structural motif of edge-sharing BO_4-tetrahedra and new compositions. In the last years, the transition metal borates came into the focus of our research activities, e.g. iron borates.

Under ambient-pressure conditions, five compositions are known in the system Fe–B–O, namely $Fe^{II}Fe^{III}(BO_3)O$ (*Pmcn*: Warwickite-structure [18,19], $P2_1/c$: distorted Warwickite-structure [18,20]), $Fe^{II}_2Fe^{III}(BO_3)O_2$ (Ludwigite [20,21], Vonsenite [22,23], Hulsite [24]), $Fe^{II}Fe^{III}_2(BO_4)O_2$ (Norbergite-structure) [25,26], $FeBO_3$ [27], and FeB_4O_7 [28,29]. $Fe^{II}Fe^{III}_2(BO_4)O_2$ consists of isolated BO_4-tetrahedra and, like $Fe^{II}Fe^{III}(BO_3)O$ and $Fe^{II}_2Fe^{III}(BO_3)O_2$, of isolated oxygen-atoms. In FeB_4O_7, both trigonal planar and tetrahedral building blocks can be found. All other compounds ($FeBO_3$, the polymorphic phases of $Fe^{III}Fe^{II}(BO_3)O$, and $Fe^{II}_2Fe^{III}(BO_3)O_2$) are exclusively built up from trigonal planar BO_3-groups. In this sense, the application of high-pressure conditions to borates with BO_3-groups could lead to new iron borates, exhibiting an increased portion of BO_4-tetrahedra due to the pressure coordination rule [30]. E.g., in $FeBO_3$, an isostructural first-order phase transition under high-pressure conditions (diamond anvil cell; $p = 53 \pm 2$ GPa), described in the same space group, is referred [31,32].

In this publication, we report the synthesis and structural details of the new high-pressure iron borate α-FeB_2O_4.

2. Experimental section

The new high-pressure phase α-FeB_2O_4 was prepared via a high-temperature/high-pressure synthesis, starting from the binary oxides Fe_2O_3 and B_2O_3.

A mixture of Fe_2O_3 (Sigma-Aldrich Chemie GmbH, Munich, Germany, 99.9%) and B_2O_3 (Strem Chemicals, Newburyport, USA, >99.9%) at a ratio of 1:1 was ground up and filled into a boron nitride crucible (Henze BNP GmbH, HeBoSint® S10, Kempten, Germany). This crucible was placed into the center of an 18/11 - assembly, which was compressed by eight tungsten carbide cubes (TSM-10 Ceratizit, Reutte, Austria). The details of preparing the assembly can be looked up in Refs. [33–37]. Pressure was applied by a multianvil device, based on a Walker-type module, and a 1000 ton press (both devices from the company Voggenreiter, Mainleus, Germany). The sample was compressed to 7.5 GPa for 3 h, then heated to 1100 °C for 10 min and kept there for 5 min. Afterwards, the sample was cooled down to 750 °C in 15 min, followed by quenching to room temperature after switching off the heating. Decompression occurred during a period of 9 h. The

* Corresponding author. Fax: +43 512 507 2934.
E-mail address: hubert.huppertz@uibk.ac.at (H. Huppertz).

0022-4596/$ - see front matter © 2008 Elsevier Inc. All rights reserved.
doi:10.1016/j.jssc.2008.05.016

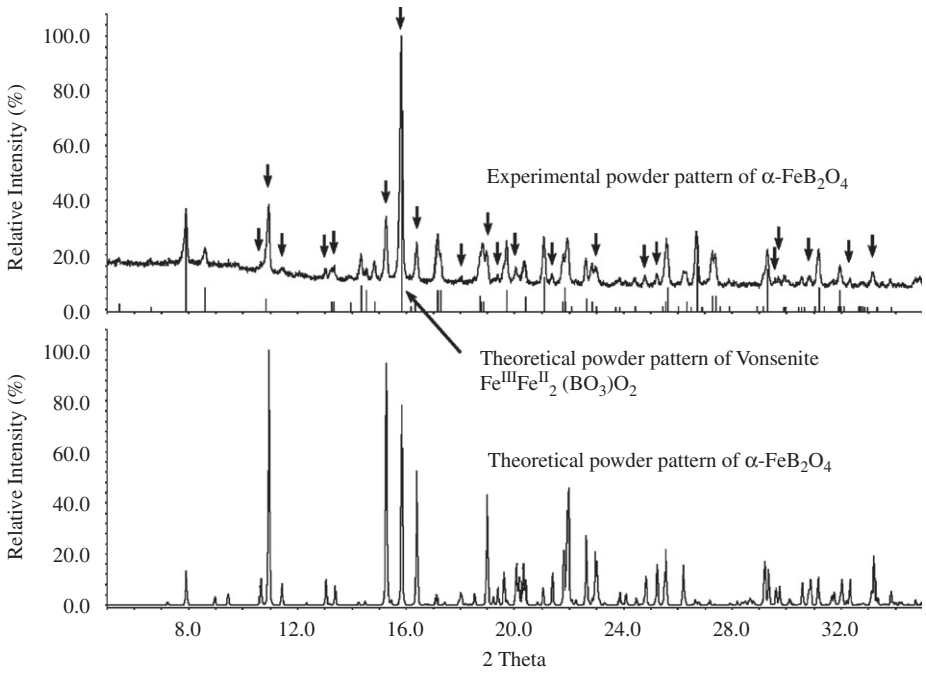

Fig. 1. Experimental powder pattern (top, black), compared with a theoretical powder pattern of Vonsenite $Fe^{II}_2Fe^{III}(BO_3)O_2$ (top, gray), and a theoretical powder pattern of α-FeB_2O_4 (bottom, black). Arrows mark explicit reflections of α-FeB_2O_4.

recovered experimental MgO-octahedron (pressure transmitting medium) was broken apart and the sample carefully separated from the surrounding boron nitride crucible, releasing the colorless, crystalline compound α-FeB_2O_4, dispersed with black needles coming from the normal-pressure iron oxide borate Vonsenite $Fe^{II}_2Fe^{III}(BO_3)O_2$. All attempts to gain a pure sample of α-FeB_2O_4 resulted in a mixture of several different phases. Fig. 1 shows a typical powder pattern of the sample (top), exhibiting α-FeB_2O_4 and a remarkable amount of Vonsenite. The graphic displays the experimental powder pattern of the sample, compared with a theoretical powder pattern of Vonsenite $Fe^{II}_2Fe^{III}(BO_3)O_2$ (top) and a theoretical powder pattern of α-FeB_2O_4 (bottom). Arrows in the experimental powder pattern indicate explicit reflections of α-FeB_2O_4. Due to the fact that α-FeB_2O_4 possesses iron in the oxidation state +II, the iron cations from the starting material Fe_2O_3 must be reduced from +III to +II. From our experimental experience we know about the reducing conditions in our high-pressure assembly, especially at high temperatures. We often observe metallic impurities (the corresponding metals of the oxides) at the border of the crucible and in the sample, when the temperature for the synthesis of a borate was too high. We suppose that the boron nitride of our crucible plays an important role in these reactions. Details about the reaction mechanism are still unknown.

3. Crystal structure analysis

For the crystal structure analysis, a small single crystal of α-FeB_2O_4 was isolated by mechanical fragmentation and examined through a Buerger camera, equipped with an image plate system (Fujifilm BAS–1800) in order to establish both symmetry and suitability for an intensity data collection. The single crystal intensity data were measured at room temperature by a Stoe IPDS–I diffractometer with graphite monochromatized Mo$K\alpha$ ($\lambda = 71.073$ pm) radiation. A numerical absorption correction was applied with the program Habitus [38]. Table 1 shows all relevant details of the data collection and evaluation. Structure solution and parameter refinement (full-matrix least squares against F^2) were successfully performed, using the SHELX-97 software suite [39,40] with anisotropic atomic displacement parameters for all atoms. According to the systematic extinctions *with $l \neq 2n$, $0k0$ with $k \neq 2n$, and $00l$ with $l \neq 2n$, the monoclinic space group $P2_1/c$ (no. 14) was derived. The final difference Fourier syntheses did not reveal any significant residual peaks in all refinements. The positional parameters of the refinements, anisotropic displacement parameters, interatomic distances, and interatomic angles are listed in Tables 2–5. Further information of the crystal structure is available from the Fachinformationszentrum Karlsruhe, D–76344 Eggenstein–Leopoldshafen (Germany), by quoting the Registry no. CSD–419183.*

The powder diffraction pattern (Fig. 1) was obtained in transmission geometry from a flat sample of the reaction product, using a STOE STADI P powder diffractometer with monochromatized Mo$K\alpha_1$ radiation. The diffraction pattern was indexed with the program ITO [41] on the basis of a monoclinic unit cell. The calculation of the lattice parameters (Table 1) was founded on least-square fits of the powder data. The correct indexing of the patterns of α-FeB_2O_4 was confirmed by intensity calculations, taking the atomic positions from the structure refinement. The lattice parameters, determined from the powder data and single crystal data, fit well.

4. Results and discussion

Fig. 2 gives a view of the crystal structure of α-FeB_2O_4 along [1 0 0]. The high-pressure phase is built up exclusively of corner-sharing BO_4-tetrahedra, interconnected to condensed borate layers (Fig. 3). These layers consist of six-membered rings, forming channels along [1 0 0], in which the iron cations are arranged. Considering the orientation of the tetrahedra, building up one ring, only one type of ring with the topology UUDUDD (U = up, D = down) is found (Fig. 4). β-$SrGa_2O_4$ [42], the high-pressure phase $CaAl_2O_4$-II [43,44], and $CaGa_2O_4$ [45] reveal the analogous orientation of tetrahedra and the same connection of

Table 1
Crystal data and structure refinement of α-FeB_2O_4

Empirical formula	FeB_2O_4
Molar mass/g mol^{-1}	141.47
Crystal system	Monoclinic
Space group	$P2_1/c$
Lattice parameters from powder data	
Radiation	Mo$K\alpha_1$ ($\lambda = 71.073$ pm)
a/pm	715.2 (2)
b/pm	745.8 (4)
c/pm	861.7 (3)
β/°	94.78 (4)
Volume/nm^3	0.4580 (3)
Single crystal diffractometer	Stoe IPDS-I
Radiation	Mo$K\alpha$ ($\lambda = 71.073$ pm)
Single crystal data	
a/pm	715.2 (2)
b/pm	744.5 (2)
c/pm	862.3 (2)
β/°	94.71 (3)
Volume/nm^3	0.4576 (2)
Formula units per cell	$Z = 8$
Temperature/K	293 (2)
Calculated density/g cm^{-3}	4.107
Crystal size/mm^3	$0.096 \times 0.052 \times 0.026$
Absorption coefficient/mm^{-1}	6.352
F (0 0 0)	544
θ range/°	$2.7 \leqslant \theta \leqslant 30.5$
Range in $h\,k\,l$	± 10, ± 10, $-12/10$
Total no. reflections	4732
Independent reflections	1376 ($R_{int} = 0.0293$)
Reflections with $I > 2\sigma(I)$	1060 ($R_\sigma = 0.0291$)
Data/parameters	1376/128
Absorption correction	Numerical (HABITUS [38])
Transm. ratio (min/max)	0.6218/0.7529
Goodness-of-fit (F^2)	0.909
Final R indices ($I > 2\sigma(I)$)	R1 = 0.0226
	wR2 = 0.0509
R indices (all data)	R1 = 0.0350
	wR2 = 0.0532
Extinction coefficient	0.021 (2)
Largest differ. peak, deepest hole/eÅ^{-3}	0.503/−0.621

Table 2
Atomic coordinates (*Wyckoff* site 4*e* for all atoms) and isotropic equivalent displacement parameters (U_{eq}/Å^2) for α-FeB_2O_4 (space group: $P2_1/c$)

Atom	x	y	z	U_{eq}
Fe1	0.02841 (4)	0.22840 (4)	0.10878 (4)	0.0063 (2)
Fe2	0.47421 (4)	0.26064 (4)	0.14062 (4)	0.0076 (2)
B1	0.7007 (3)	0.1032 (3)	0.8840 (3)	0.0047 (4)
B2	0.6798 (3)	0.9036 (3)	0.1207 (3)	0.0040 (4)
B3	0.1995 (3)	0.4359 (3)	0.8603 (3)	0.0052 (4)
B4	0.8193 (3)	0.4290 (3)	0.8581 (3)	0.0044 (4)
O1	0.2320 (2)	0.2479 (2)	0.2960 (2)	0.0051 (3)
O2	0.2355 (2)	0.0583 (2)	0.0267 (2)	0.0052 (3)
O3	0.5148 (2)	0.1620 (2)	0.9236 (2)	0.0053 (3)
O4	0.0038 (2)	0.0174 (2)	0.3061 (2)	0.0069 (3)
O5	0.8327 (2)	0.2506 (2)	0.9282 (2)	0.0049 (3)
O6	0.6832 (2)	0.4344 (2)	0.2157 (2)	0.0051 (3)
O7	0.6822 (2)	0.0602 (2)	0.2218 (2)	0.0063 (3)
O8	0.2370 (2)	0.4319 (2)	0.0286 (2)	0.0061 (3)

U_{eq} is defined as one third of the trace of the orthogonalized U_{ij} tensor.

Table 3
Anisotropic displacement parameters (U_{ij}/Å^2) for α-FeB_2O_4 (space group $P2_1/c$)

Atom	U_{11}	U_{22}	U_{33}	U_{23}	U_{13}	U_{12}
Fe1	0.0054 (2)	0.0073 (2)	0.0058 (2)	−0.0002 (2)	−0.0021 (2)	0.0009 (2)
Fe2	0.0054 (2)	0.0104 (2)	0.0069 (2)	−0.0043 (2)	−0.0005 (2)	0.00075 (9)
B1	0.005 (2)	0.0051 (9)	0.004 (2)	0.0007 (8)	−0.0003 (8)	0.0004 (7)
B2	0.003 (2)	0.0052 (9)	0.003 (2)	−0.0002 (8)	−0.0007 (8)	0.0001 (7)
B3	0.007 (2)	0.0039 (9)	0.004 (2)	0.0000 (7)	−0.0001 (8)	−0.0002 (7)
B4	0.004 (2)	0.0048 (9)	0.004 (2)	−0.0001 (7)	0.0005 (8)	0.0010 (7)
O1	0.0082 (7)	0.0038 (7)	0.0032 (8)	−0.0001 (5)	−0.0007 (6)	−0.0007 (4)
O2	0.0063 (7)	0.0045 (6)	0.0051 (8)	0.0009 (5)	0.0017 (6)	0.0014 (5)
O3	0.0032 (7)	0.0056 (6)	0.0072 (8)	−0.0019 (5)	−0.0001 (5)	−0.0002 (5)
O4	0.0041 (7)	0.0080 (6)	0.0087 (8)	−0.0026 (5)	0.0008 (5)	−0.0002 (5)
O5	0.0044 (7)	0.0048 (6)	0.0053 (7)	0.0014 (5)	−0.0009 (5)	−0.0004 (4)
O6	0.0044 (7)	0.0064 (6)	0.0044 (8)	−0.0001 (5)	−0.0002 (6)	−0.0019 (5)
O7	0.0061 (7)	0.0067 (6)	0.0057 (8)	−0.0016 (5)	−0.0010 (6)	0.0015 (5)

Table 4
Interatomic distance /pm in α-FeB_2O_4, calculated with the single-crystal lattice parameters

Fe1-O5	201.3 (2)	Fe2-O6	204.1 (2)
Fe1-O1	208.8 (2)	Fe2-O3	205.3 (2)
Fe1-O2	211.4 (2)	Fe2-O7	218.1 (2)
Fe1-O8	227.3 (2)	Fe2-O8	227.3 (2)
Fe1-O4a	229.1 (2)	Fe2-O1	227.8 (2)
Fe1-O4b	233.3 (2)	Fe2-O2	242.3 (2)
	∅ = 218.5	Fe2-O3	250.1 (2)
			∅ = 225.0
B1-O3	146.6 (3)	B3-O8	145.4 (3)
B1-O6	147.3 (3)	B3-O6	146.9 (3)
B1-O5	147.7 (3)	B3-O4	148.0 (3)
B1-O2	148.0 (3)	B3-O1	150.2 (3)
	∅ = 147.4		∅ = 147.6
B2-O7	145.5 (3)	B4-O5	145.9 (3)
B2-O1	147.7 (3)	B4-O7	147.0 (3)
B2-O2	148.0 (3)	B4-O4	148.3 (3)
B2-O3	149.5 (3)	B4-O8	150.1 (3)
	∅ = 147.7		∅ = 147.8

Table 5
Interatomic angles /° in α-FeB_2O_4, calculated with the single-crystal lattice parameters

O3-B1-O5	106.9 (2)	O1-B2-O3	102.7 (2)
O3-B1-O6	106.3 (2)	O2-B2-O3	106.4 (2)
O5-B1-O2	107.8 (2)	O7-B2-O1	110.7 (2)
O6-B1-O2	110.9 (2)	O7-B2-O2	112.0 (2)
O3-B1-O2	111.6 (2)	O1-B2-O2	112.3 (2)
O6-B1-O5	113.3 (2)	O7-B2-O3	112.3 (2)
	∅ = 109.5		∅ = 109.4
O6-B3-O4	105.4 (2)	O7-B4-O8	106.6 (2)
O4-B3-O1	105.6 (2)	O7-B4-O4	107.2 (2)
O6-B3-O1	108.8 (2)	O4-B4-O8	107.7 (2)
O8-B3-O1	109.2 (2)	O5-B4-O4	109.9 (2)
O8-B3-O6	113.2 (2)	O5-B4-O8	111.8 (2)
O8-B3-O4	114.4 (2)	O5-B4-O7	113.4 (2)
	∅ = 109.4		∅ = 109.4

the layers. α-FeB_2O_4 is isotypic to these compounds. The orthorhombic compound $BaFe_2O_4$ [46] shows the same topology, but the layers are interconnected in a different way, resulting in a different crystal structure.

Drawing a comparison to other network structures of tetrahedra, a close relationship to the new high-pressure borate CdB_2O_4 [10] can be discovered. The network structure consists also of corner-sharing BO_4-tetrahedra, which are linked to condensed layers of six-membered rings. In CdB_2O_4, these rings show a staged adjustment, in which one fourth of the rings reveal

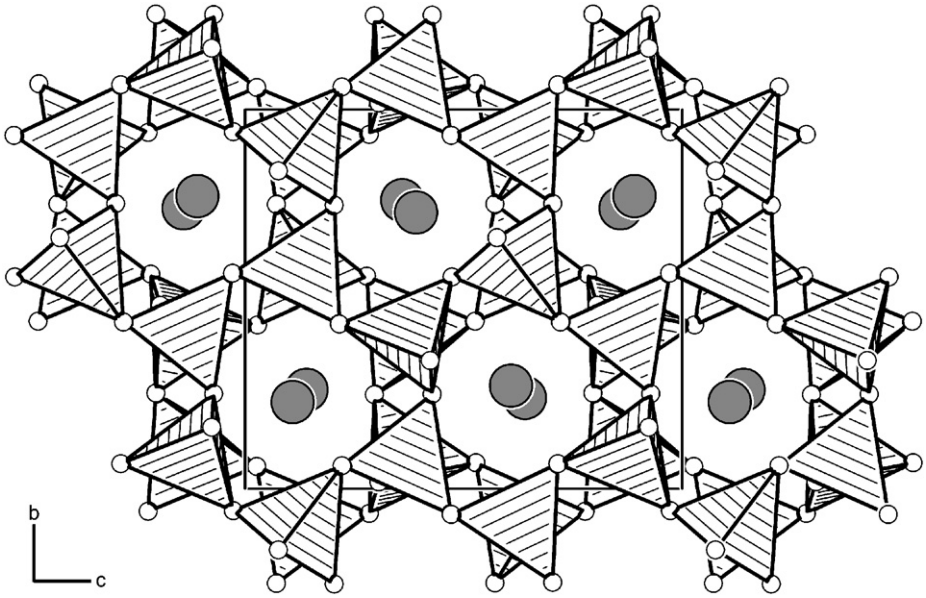

Fig. 2. Crystal structure of α-FeB_2O_4 along [1 0 0], exhibiting layers of six-membered rings of corner-sharing BO_4-tetrahedra and Fe^{2+} ions.

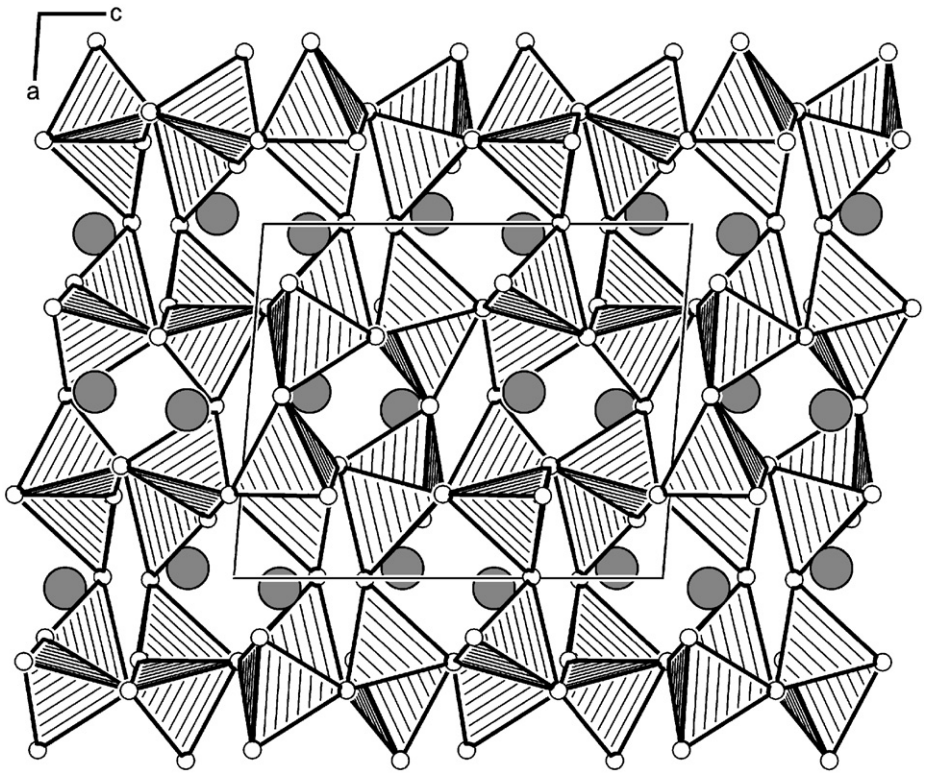

Fig. 3. View of the condensed borate layers in α-FeB_2O_4 along [0 1 0].

an UDUDUD topology and the remaining rings an UUUDDD topology (Fig. 5). In contrast, α-FeB_2O_4 exhibits only one kind of orientation (UUDUDD). So, all the mentioned compounds can be understood as stuffed derivates of the Tridymite framework-structure.

The B–O bond lengths in α-FeB_2O_4 (Table 4) vary between 145 and 150 pm with an average B–O bond length of 146.3 pm, which tallies well to the known average value of 147.6 pm for borates [47,48]. The O–B–O angles in the four crystallographically independent BO_4-tetrahedra range between 102.7° and 114.4° (Table 5) with a mean value of 109.4°. The Fe–O distances for the sixfold coordinated iron cations (Fe1; Fig. 6 left) change from 201 to 233 pm with a mean value of 218.5 pm. This value is slightly higher than the average Fe–O distance of sixfold coordinated iron atoms in $Fe^{II}Fe^{III}_2(BO_4)O_2$ (203.8 pm) or in $FeBO_3$ (202.8 pm). For the sevenfold coordinated iron atoms (Fe2; Fig. 6 right), the Fe–O bond lengths vary from 204 to 250 pm with a mean value of

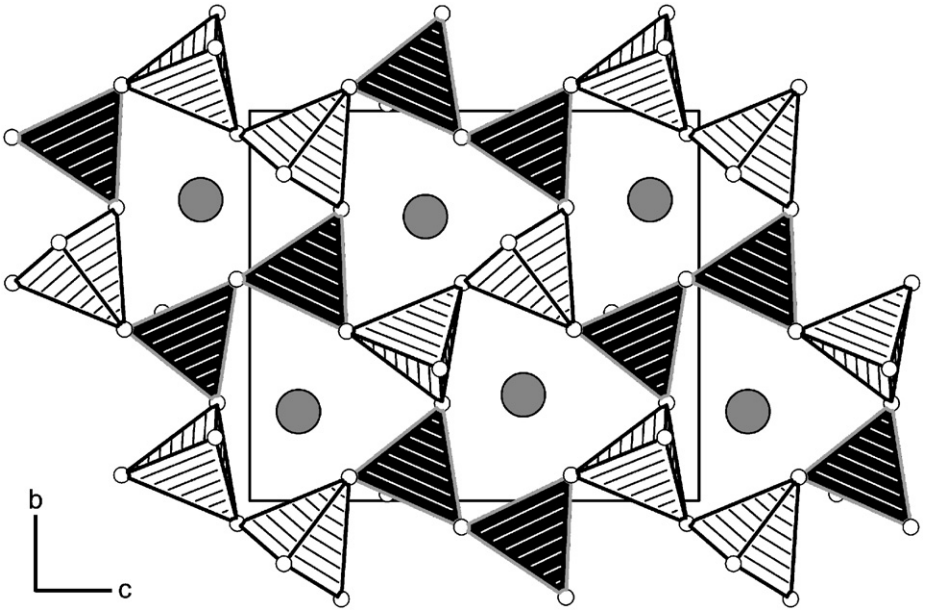

Fig. 4. Single layer of BO_4-tetrahedra in α-FeB_2O_4, built up from six-membered rings with the topology UUDUDD (light-shaded BO_4-tetrahedra face upwards (U), dark-shaded tetrahedra downwards (D)) with a view along [1 0 0].

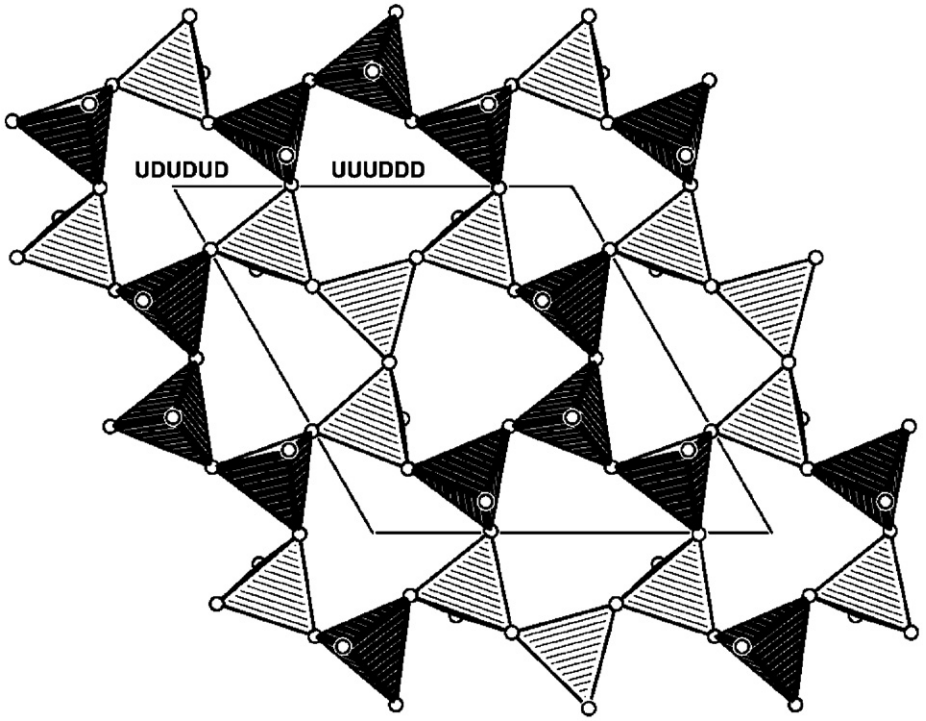

Fig. 5. Single layer of BO_4-tetrahedra in CdB_2O_4, built up from two different types of six-membered rings (UDUDUD, UUUDDD). White spheres represent O-atoms. Light-shaded BO_4-polyhedra face downwards (D), dark-shaded polyhedra face upwards (U) (view along [0 0 $\bar{1}$]).

225 pm, which is larger than the Fe–O distances for Fe1 due to the higher coordination number.

Then, we calculated bond-valence sums for α-FeB_2O_4, supported by the bond-length/bond-strength (ΣV) and the CHARDI concept (ΣQ) (Table 6). [49–51] The formal ionic charges of the atoms, acquired by X-ray structure analysis, were in agreement within the limits of the concepts. Furthermore, we calculated the Madelung part of lattice energy (MAPLE) values [52–54] for α-FeB_2O_4 in order to compare them with MAPLE values of the binary components FeO (Wuestit) and the high-pressure modification B_2O_3-II. The reason for that is the additive potential of the MAPLE-values, which makes it possible to calculate hypothetical values for α-FeB_2O_4, starting from binary oxides. As a result, we obtained a value of 26474 kJ/mol in comparison to 26427 kJ/mol (deviation: 0.2%), starting from the binary oxides [1 × FeO (4489 kJ/mol) + 1 × B_2O_3-II (21938 kJ/mol)].

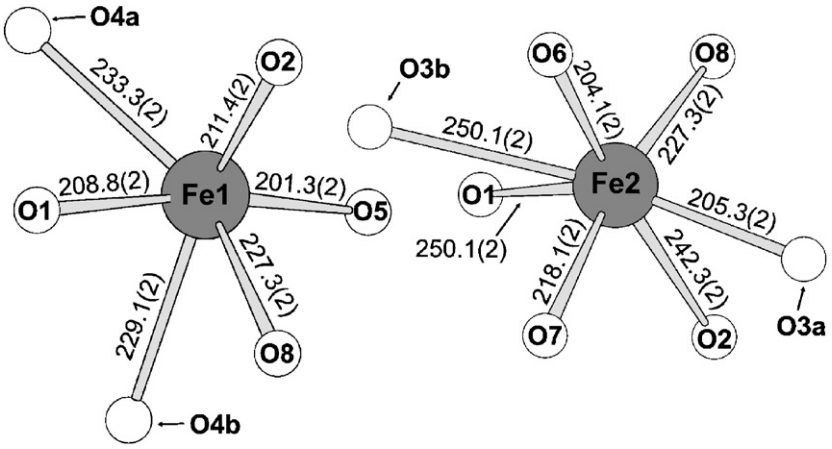

Fig. 6. Coordination spheres of the Fe^{2+} ions. Iron – oxygen distances are shown in pm.

Table 6
Charge distribution in α-FeB_2O_4, calculated with the bond-length/bond-strength concept (ΣV) [49,50] and the CHARDI concept (ΣQ) [51]

	Fe1	Fe2	B1	B2	B3	B4		
ΣQ	1.87	1.90	3.03	3.01	3.01	3.00		
ΣV	1.99	1.99	2.96	2.98	3.02	3.05		
	O1	O2	O3	O4	O5	O6	O7	O8
ΣQ	−2.07	−2.00	−2.05	−1.90	−2.01	−1.96	−1.86	−1.97
ΣV	−2.10	−2.01	−2.02	−1.88	−2.07	−2.01	−1.93	−1.98

5. Conclusions

In this article, we described the synthesis and crystal structure of the new high-pressure phase α-FeB_2O_4. It represents a high-pressure iron borate, isotypic to the compounds β-$SrGa_2O_4$ [42], $CaAl_2O_4$-II [43,44], and $CaGa_2O_4$ [45], and exhibits a new composition in the ternary system Fe–B–O. This is an impressive example of the efficiency of high-pressure/high-temperature synthesis, revealing recent compositions with new structures. In the last days, we were able to synthesize a second phase in the system Fe–B–O [55]. The structural analysis of this compound exhibited the same composition but a different structure. The structure of this new iron borate, designated now as β-FeB_2O_4, is isotypic to HP-NiB_2O_4 [17].

Acknowledgments

We thank Thomas Miller (LMU München) for collecting the single-crystal data. Special thanks go to Prof. Dr. W. Schnick (LMU München) for his continuous support in these investigations. This work was financially supported by the Deutsche Forschungsgemeinschaft (HU 966/2-3) and the Fonds der Chemischen Industrie.

References

[1] J.S. Knyrim, J. Friedrichs, S. Neumair, F. Roeßner, Y. Floredo, S. Jakob, D. Johrendt, R. Glaum, H. Huppertz, Solid State Sci. 10 (2007) 168.
[2] H. Huppertz, G. Heymann, Solid State Sci. 5 (2003) 281.
[3] H. Huppertz, Z. Naturforsch. B 58 (2003) 257.
[4] H. Emme, M. Weil, H. Huppertz, Z. Naturforsch. B 60 (2005) 815.
[5] G. Heymann, T. Soltner, H. Huppertz, Solid State Sci. 8 (2006) 821.
[6] A. Haberer, G. Heymann, H. Huppertz, Z. Naturforsch. B 62 (2007) 759.
[7] J.S. Knyrim, P. Becker, D. Johrendt, H. Huppertz, Angew. Chem. 118 (2006) 8419
Angew. Chem. Int. Ed. 45 (2006) 8239.
[8] J.S. Knyrim, F.M. Schappacher, R. Pöttgen, J. Schmedt auf der Günne, D. Johrendt, H. Huppertz, Chem. Mater. 19 (2007) 254.
[9] A. Haberer, G. Heymann, H. Huppertz, J. Solid State Chem. 180 (2007) 1595.
[10] J.S. Knyrim, H. Emme, M. Döblinger, O. Oeckler, M. Weil, H. Huppertz, Chem. Eur. J. 14 (2008), doi:10.1002/chem.200800506.
[11] H. Huppertz, B. von der Eltz, J. Am. Chem. Soc. 124 (2002) 9376.
[12] H. Huppertz, Z. Naturforsch. B 58 (2003) 278.
[13] H. Huppertz, H. Emme, J. Phys.: Condens. Matter 16 (2004) 1283.
[14] H. Emme, H. Huppertz, Z. Anorg. Allg. Chem. 628 (2002) 2165.
[15] H. Emme, H. Huppertz, Chem. Eur. J. 9 (2003) 3623.
[16] H. Emme, H. Huppertz, Acta Crystallogr. C 61 (2005) i29.
[17] J.S. Knyrim, F. Roeßner, S. Jakob, D. Johrendt, I. Kinski, R. Glaum, H. Huppertz, Angew. Chem. 119 (2007) 9256
Angew. Chem. Int. Ed. 46 (2007) 9097.
[18] J.P. Attfield, A.M.T. Bell, L.M. Rodriguez-Martinez, J.M. Greneche, R. Retoux, M. Leblance, R.J. Cernik, J.F. Clarke, D.A. Perkins, J. Mater. Chem. 9 (1998) 205.
[19] J.P. Attfield, A.M.T. Bell, L.M. Rodriguez-Martinez, J.M. Greneche, R.J. Cernik, D.A. Perkins, Nature 369 (1998) 655.
[20] J.P. Attfield, J.F. Clarke, D.A. Perkins, Physica. B 180 & 181 (1992) 581.
[21] M. Mir, J. Janczak, Y.P. Mascarenhas, J. Appl. Crystallogr. 39 (2006) 42.
[22] M. Federico, Period. Mineral. 26 (1957) 191.
[23] J.S. Swinnea, H. Steinfink, Am. Mineral. 68 (1983) 827.
[24] N.A. Yamnova, M.A. Simonov, N.V. Belov, Kristallografiya 20 (1975) 156.
[25] J.G. White, A. Miller, R.E. Nielsen, Acta Crystallogr. 19 (1965) 1060.
[26] R. Diehl, G. Brandt, Acta Crystallogr. B 31 (1975) 1662.
[27] R. Diehl, Solid State Commun. 17 (1975) 743.
[28] T.A. Kravchuk, Y.D. Lazebnik, Russ. J. Inorg. Chem. 12 (1967) 21.
[29] I.M. Rumanova, E.A. Genkina, N.V. Belov, Kim. Ser. 5 (1981) 571.
[30] A. Neuhaus, Chimia 18 (1964) 93.
[31] A.G. Gavriliuk, I.A. Trojan, R. Boehler, M. Ermets, A. Zerr, I.S. Lyubutin, V.A. Sarkisyan, JETP Lett. 75 (2002) 23.
[32] K. Parlinski, Eur. Phys. J. B 27 (2002) 283.
[33] D. Walker, M.A. Carpenter, C.M. Hitch, Am. Mineral. 75 (1990) 1020.
[34] D. Walker, Am. Mineral. 76 (1991) 1092.
[35] H. Huppertz, Z. Kristallogr. 219 (2004) 330.
[36] D.C. Rubie, Phase Transitions 68 (1999) 431.
[37] N. Kawai, S. Endo, Rev. Sci. Instrum. 8 (1970) 1178.
[38] W. Herrendorf, H. Bärnighausen, HABITUS—program for numerical absorption correction, University of Karlsruhe/Giessen, Germany, 1993/1997.
[39] G.M. Sheldrick, SHELXS-97 and SHELXL-97, Program suite for the solution and refinement of crystal structures, University of Göttingen, Göttingen, Germany, 1997.
[40] G.M. Sheldrick, Acta Crystallogr. A 64 (2008) 112.
[41] J.W. Visser, J. Appl. Crystallogr. 2 (1969) 89.
[42] V. Kahlenberg, R.X. Fischer, C.S.J. Shaw, J. Solid State Chem. 153 (2000) 294.
[43] S. Ito, K. Suzuki, M. Iagaki, S. Naka, Mater. Res. Bull. 15 (1980) 925.
[44] B. Lazic, V. Kahlenberg, J. Konzett, Z. Kristallogr. 222 (2007) 690.
[45] H.J. Deiseroth, Hk. Müller-Buschbaum, Z. Anorg. Allg. Chem. 402 (1973) 201.
[46] W. Leib, Hk. Müller-Buschbaum, Z. Anorg. Allg. Chem. 538 (1986) 71.
[47] F.C. Hawthorne, P.C. Burns, J.D. Grice, Reviews in mineralogy. In Boron: Mineralogy, Petrology, and Geochemistry; Mineralogical Society of America: Washington DC, 1996, Chapter 2, Vol. 33.
[48] E. Zobetz, Z. Kristallogr. 191 (1990) 45.
[49] I.D. Brown, D. Altermatt, Acta Crystallogr. B 41 (1985) 244.

[50] N.E. Brese, M. O'Keeffe, Acta Crystallogr. B 47 (1991) 192.
[51] R. Hoppe, S. Voigt, H. Glaum, J. Kissel, H.P. Müller, K.J. Bernet, Less-Common Met. 156 (1989) 105.
[52] R. Hoppe, Angew. Chem. 78 (1966) 52
Angew. Chem. Int. Ed. 5 (1966) 96.
[53] R. Hoppe, Angew. Chem. 82 (1970) 7
Angew. Chem. Int. Ed. 9 (1970) 25.
[54] R. Hübenthal, MAPLE—Program for the Calculation of MAPLE Values, Vers. 4, University of Gießen, Gießen, Germany, 1993.
[55] S. Neumair, H. Huppertz, personal communication.